J. Fluid Mech. (2005), *vol.* 527, *pp.* 285–301.
DOI: 10.1017/S002211200400312X Printed in the United Kingdom

Free-surface horizontal waves generated by low-frequency alternating magnetic fields

By Y. FAUTRELLE, J. ETAY AND S. DAUGAN

Institut National Polytechnique de Grenoble-CNRS-EPM, ENSHMG, BP 95, 38402 Saint Martin d'Hères cedex, France

(Received 7 September 2001 and in revised form 6 May 2004)

New types of electromagnetic parametric instability have been observed at the periphery of the free surface of a liquid metal pool in the presence of a low-frequency magnetic field. An experimental set-up is used to observe the motion of a mercury layer on a substrate located in a solenoidal coil supplied with low-frequency alternating electric currents. The Lorentz body forces produced are mainly oscillatory and generate motion in the liquid. Various regular and irregular free-surface patterns are observed. Two-dimensional stability analysis shows that axisymmetric waves are directly forced by the electromagnetic forces while azimuthal waves are the result of instability. The experimental stability diagram exhibits 'tongues' as already observed for parametric resonance instability. For high magnetic field strengths, the free-surface patterns become highly unstructured. High-amplitude 'fingers' as well as solitary waves are observed. Measurements of the deformation observed on photographs are compared with rough theoretical estimates.

1. Introduction

When a liquid metal pool is subjected to an a.c. magnetic field, electrical currents are induced in the liquid metal and interact with the applied magnetic field to create electromagnetic body forces referred to as Lorentz forces. These Lorentz forces are composed of a mean value (time averaged) and an oscillating part that has a frequency twice that of the magnetic field. They are responsible for both bulk motion and free-surface deformation. Such phenomena are encountered in many metallurgical applications such as electromagnetic stirring and levitation or quasi-levitation of liquid metals. For very low applied magnetic field frequencies, the mean value of the electromagnetic forces is negligible compared to the oscillating component (Taberlet & Fautrelle 1985). Moreover, at low frequencies, the oscillating part is irrotational and does not directly drive any liquid motion (Galpin & Fautrelle 1992, hereinafter referred to as GF92). However, the oscillating force modifies the pressure field and may in this way be indirectly responsible for free-surface motion. It has been shown experimentally in GF92 that a uniform vertical low-frequency magnetic field (typically a few Hertz) can generate various types of wave at the surface of a 200 mm-diameter mercury pool. Galpin, Fautrelle & Sneyd (1992, hereinafter referred to as GFS92) used theoretical stability analysis to show that both forced axisymmetric waves as well as non-symmetric waves, resulting from parametric-type instabilities, were excited.

From a practical viewpoint, such phenomena may be useful in various metallurgical processes. In ladle metallurgy for example, stirring of the free surface could be used to produce the enhanced mass transfer across the liquid metal interface required to

Density $\rho(\mathrm{kg\,m^{-3}})$	Surface tension $\gamma(\mathrm{N\,m^{-1}})$	Viscosity $\nu(\mathrm{m^2\,s^{-1}})$	Electrical conductivity $\sigma(\Omega\ \mathrm{m^{-1}})$
13590	0.485	10^{-7}	10^{6}

TABLE 1. Physical properties of the mercury at room temperature.

eliminate undesirable substances. In continuous casting of steel, electromagnetically driven oscillation of the surface meniscus near the triple point, i.e. the area where slag, liquid metal and solid metal are in contact, could partially replace mechanical mould oscillation (Li, Sassa & Asai 1994).

We will study the behaviour of a thin pool of mercury subjected to a vertical low-frequency magnetic field. The present paper is an extension of a previous preliminary investigation (Daugan, Fautrelle & Etay 1999). The initial aim was to analyse the free-surface motion by enhancing the electromagnetically driven horizontal motion and minimizing the influence of gravity on the wave motion. Experiments involving oscillating liquid drops have been carried out so far. Keizer (1977) studied self-induced oscillations of a liquid mercury drop immersed in an electrolyte solution during electrochemical reactions. For a liquid metal drop subjected to a high-frequency a.c. magnetic field, typically of the order of 10 kHz, Karcher, Kocourek & Schulze (2003) showed that axisymmetric shaping can become unstable and that horizontal oscillations appear beyond a magnetic field threshold. Similar free-surface patterns were investigated by Yoshiyasu, Matsuda & Takaki (1996) who focused on the motion of a water drop on a vibrating plate. They observed regular surface waves, but it was not possible to reach unstructured patterns. The surface motion was attributed to a parametric instability. The present experiment is very similar to that carried out by Yoshiyasu *et al.* (1996). We independently control the magnetic field amplitude and frequency. Moreover, large magnetic field amplitude may be used, providing a wider variety of phenomena.

The experimental set-up is described in § 2. Rough theoretical estimates of the characteristics concerned are presented in § 3, the experimental results in § 4 and a discussion of the results and conclusions in § 5.

2. Experimental set-up

The experimental apparatus is illustrated in figure 1. The mercury (physical properties listed in table 1) pool is set up on a Plexiglas substrate located inside a coil. The coil is supplied with single-phase a.c. electric currents with frequencies varying between 1 and 10 Hz. The dimensions of the coil are detailed in figure 1(*a*). The number of turns is 500. In the centre of the coil, the magnetic field may be considered to be uniform to within 1 %. The magnetic field strength B_0 (maximum value) is proportional to the coil current I (r.m.s. value), and the experimental proportionality coefficient is 0.0024 ± 0.0001 in SI units. The accuracy is ± 3A.

The pool has a circular shape at rest. Its size is defined by the outer radius a, as shown in figure 1(*c*). It is determined by direct measurements with an accuracy of ± 1 mm. In order to centre the pool, the substrate has a slightly conical shape (figure 1(*b*). The cone angle α is equal to 1.745×10^{-2} rad. The radius a of the pool at rest may be varied from 10 to 40 mm. Its apparent height h, as defined in figure 1(*c*), depends on the value of the radius owing to the slightly conical shape of the substrate.

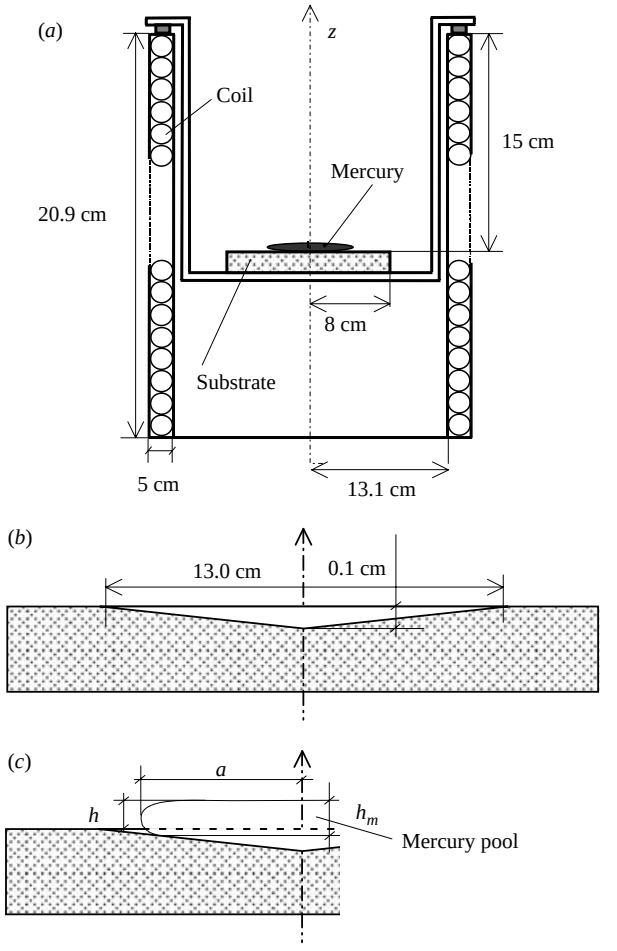

FIGURE 1. Sketch of the apparatus: (*a*) overall view, (*b*) detailed view of the substrate, (*c*) detailed view of the mercury pool.

Pool radius a (mm)	Pool height h (mm)	Meniscus height h_m (mm)
20	2.28 ± 0.10	3.17 ± 0.20
30	2.64	3.36
40	3.01	3.47

TABLE 2. Experimental values of the pool height as a function of radius.

The value of h has been measured by photographic analysis for various radii and the results are presented in table 2. The observations of the meniscus indicate that the contact angle is almost 180°. Therefore, the mercury does not wet the present substrate. The actual meniscus height h_m is somewhat higher than the value of h (see for example figure 1*c*). By means of a simple geometrical correction, we may deduce the value of h_m from h. The results are given in table 2.

The meniscus shape at rest has not been calculated. However, from Davies & Rideal (1963), Padday (1969) and Yoshiyasu *et al.* (1996), it is easy to obtain an estimate of

FIGURE 2. View of a defect in the azimuthal pattern owing to the contact between the liquid metal pool and the substrate (the initial drop radius is $a = 30\,\text{mm}$, $f = 8.050\,\text{Hz}$, $I = 140$ A).

the pool height h_e for the two-dimensional case corresponding approximately to the large values of the radius. This estimate involves the capillary length d as follows:

$$h_e \approx 2d \approx 3.81\,\text{mm with } d = \left(\frac{\gamma}{\rho g}\right)^{1/2}, \tag{1}$$

where ρ, γ and g are the liquid density, surface tension and gravity, respectively.

The above estimate is higher than the experimental meniscus heights h_m of table 2.

The pool motion is observed by video recording and image processing. The recording frequency is 25 images per second.

Special attention has been paid to the reproducibility of the experiments. Electromagnetic forces produce motion in the liquid pool on the substrate and therefore the surface properties of the latter play a relevant role in the motion. We have checked that the wetting of the mercury on the Plexiglas substrate was very weak. However, for smooth surfaces, the pool seems to stick on the substrate, and the experiments are not reproducible in a satisfactory manner. Although wetting is weak, we suspect that it is related to the mobility of the triple line (mercury/substrate/air). Figure 2 shows a typical experimental example where the azimuthal-wave structure deteriorates owing to this mobility. We find that the experiments are reproducible only if the substrate surface has a significant roughness (at least around 0.05 mm). If this condition is satisfied, the sticking effects are reduced, and the pool is able to move freely on the substrate. Davies & Rideal (1963) have pointed out that the roughness of the substrate increases the effective contact angle. Oxidation of the surface, when significant, can also alter the mobility of the pool. Thus, clean mercury is used for each experiment and the duration is limited.

We have not carried out systematic investigations on this issue. From a quantitative point of view, the reproducibility has been tested by experimental determination of the stability diagram in figure 9. Let us consider, for example, mode 5, which is the most easily triggered. We assume that the limited data dispersion of the stability curve obtained from the various measurement series attests to the reproducibility of the experiments.

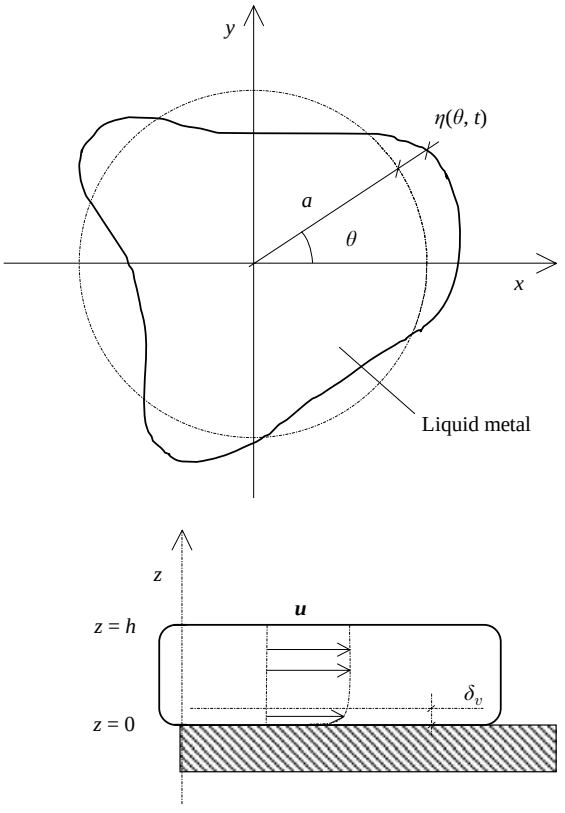

FIGURE 3. Sketch of the two-dimensional model.

3. Theoretical estimates

Estimates of the eigenfrequencies

In order to interpret the various experimental results, it is of interest to estimate the eigenfrequencies of the liquid drop. We have not tried to carry out a detailed calculation of the general case. We focus rather on its quasi-planar oscillations. For this, we use Lamb's theory (1975) applied to a simple two-dimensional pool. The liquid drop is modelled as a transverse slice of an infinite vertical cylindrical column, with a circular shape at rest. The pool is considered as a truncated cylinder parallel to the vertical z-axis. The upper free surface is assumed to be horizontal and flat (cf. figure 3). The pool free surface may oscillate freely in a horizontal plane. Then, the eigenfrequencies f_n of the free oscillations of an inviscid liquid are given by

$$f_n = \frac{\Omega_n}{2\pi} \text{ with } \Omega_n = \frac{\gamma}{\rho a^3} n(n^2 - 1), \tag{2}$$

where n denotes the mode number in the Fourier decomposition of the lateral free surface in the θ-direction of figure 3. The numerical values of f_n are given in table 3.

Dimensionless parameters

The screen parameter R_ω that measures the magnetic field created by the induced electric currents compared to the applied magnetic field $\boldsymbol{B}$ is

$$R_\omega = \mu\sigma\omega a^2, \tag{3}$$

n	1	2	3	4	5	6	7
f_n (theoretical values from (2)) (Hz)	0.0	0.448	0.896	1.417	2.004	2.652	3.354
f_n (experimental values) (Hz)	–	–	–	1.30 $\pm$0.04	1.58 $\pm$0.04	1.98 $\pm$0.03	2.30 $\pm$0.03

TABLE 3. Values of the eigenfrequencies of the liquid pool for various values of n with $a = 0.03$ m.

where μ and σ are the magnetic permeability and electrical conductivity of the mercury. In our experiment, R_ω ranges from 3×10^{-3} to 0.12. These values may be considered to be small. Thus, the applied magnetic field is weakly perturbed by the induced electric currents (see Moreau 1990, for example). Note that the parameter R_ω also represents the dimensionless frequency.

The second dimensionless parameter represents the magnetic field amplitude. In such a problem, where the free surface is driven by low-frequency magnetic fields, the effect of the magnetic field amplitude B_0 is accounted for in the interaction parameter N (see GFS92)

$$N = \frac{\sigma B_o^2}{\rho \omega}, \tag{4}$$

which may be interpreted as the ratio of electromagnetic to inertia forces.

In summary, the user-parameter space, which is formed by the magnetic field amplitude B_0 and its frequency f, may also be described by the above two dimensionless parameters N and R_ω.

Boundary layers and viscous friction

Owing to the low kinematic viscosity of mercury, we may assume that the main contribution to the viscous stresses comes from the vertical gradients of the horizontal velocity. Let us analyse the viscous effects. We assume that they are restricted to within a boundary layer of depth δ_ν smaller than the pool depth h. This assumption will be justified *a posteriori*. In the boundary layer at the bottom wall, the inertia of the fluid is balanced by two contributions, namely the electromagnetic forces and the viscous friction term. Both terms tend to decrease the fluid momentum and damp the motion.

Let us now estimate the order of magnitude of the various terms. Let η_0 be an estimate of the amplitude of the horizontal oscillating motion. The order of magnitude of the velocity field U is

$$U = \omega \eta_0. \tag{5}$$

When N is small, the Lorentz force is negligible compared to inertia. The inertia term balances the viscous term and the boundary layer is analogous to a Stokes layer. The boundary-layer thickness therefore has the classical expression (e.g. Batchelor 1967)

$$\delta_{\nu\omega} = \left(\frac{\nu}{\omega}\right)^{1/2}. \tag{6}$$

The value of $\delta_{\nu\omega}$ is usually small compared to the pool depth, as we shall see later.

When N is large, the Lorentz force balances the viscous term. The Hartmann number Ha is related to the interaction parameter by the following relation:

$$Ha^2 = \frac{\omega a^2}{\nu} N.$$

The non-dimensional parameter $\omega a^2/\nu$ is large in the present experiment. Accordingly, the Hartmann number is large. Thus, we may expect the development of a Hartmann-type boundary layer along the bottom wall. Subsequently, the expression of the boundary-layer thickness becomes (e.g. Moreau 1990)

$$\delta_{\nu B} = \frac{1}{B_0}\sqrt{\frac{\rho\nu}{\sigma}}. \tag{7}$$

From (6) and (7), we deduce the ratio between $\delta_{\nu B}$ and $\delta_{\nu\omega}$:

$$\delta_{\nu B} = \delta_{\nu\omega}/\sqrt{N}. \tag{8}$$

Thus, when the interaction parameter N is large, the Hartmann layer is thinner than the boundary layer owing to the oscillatory motion for a given value of the magnetic field angular frequency ω. The wall friction is then controlled by the magnetic field.

With the numerical values of our mercury experiment, e.g. $B_0 = 0.2T$, $f = 2$ Hz, $a = 0.03$ m, $h = 0.003$ m, $\eta_0 = 0.01$ m, the values of $\delta_{\nu\omega}$ and $\delta_{\nu B}$ are equal to 89 and 184 μm, respectively. This estimate indicates that the two boundary-layer thicknesses are comparable, since the interaction parameter is equal to 0.23 with the above numerical values. These thicknesses are significantly lower than the pool depth h.

Note that viscosity could also play an important role at the edge of the pool in the vicinity of the meniscus, and especially near the mercury–substrate–atmosphere triple point. The importance of viscosity with respect to surface tension may be estimated by means of the capillary number Ca expressed as:

$$Ca = \frac{\rho\nu U}{\gamma}, \tag{9}$$

U being a typical meniscus velocity.

The value of Ca is generally very weak in the present numerical application: $Ca = 3.4 \times 10^{-4}$. Viscous effects remain negligible near the edge of the meniscus, and inertia is likely to be balanced by surface tension deviations. This is confirmed by the order of magnitude of the Weber number that is close to unity:

$$We = \frac{\rho U^2 h}{\gamma} = 1.3. \tag{10}$$

Comparison between gravity and electromagnetic forces

In the absence of horizontal deformation of the liquid domain, GFS92 showed that the electromagnetic force $\boldsymbol{F}$ was axisymmetric and purely radial, and could be expressed as:

$$\boldsymbol{F} = -\tfrac{1}{4}\sigma\omega B_o^2 r \sin(\omega t)\boldsymbol{r}, \tag{11}$$

r and $\boldsymbol{r}$ being, respectively, a radial coordinate and a unit vector along the radial direction.

With $B_0 = 0.2$ T, $f = 2$ Hz, $r \approx a = 0.03$ m and using (11), the amplitude of the electromagnetic force can be estimated as:

$$\boldsymbol{F} \approx 3.77 \times 10^3 \text{ N m}^{-3} \tag{12}$$

Note that the amplitude of the corresponding specific gravity force is equal to

$$\rho g = 1.33 \times 10^5 \text{ N m}^{-3} \tag{13}$$

Nevertheless, because of the conicity of the substrate, the projection of the gravity body force on the lower wall is smaller and equal to 2.05×10^3 N m^{-3}. The latter

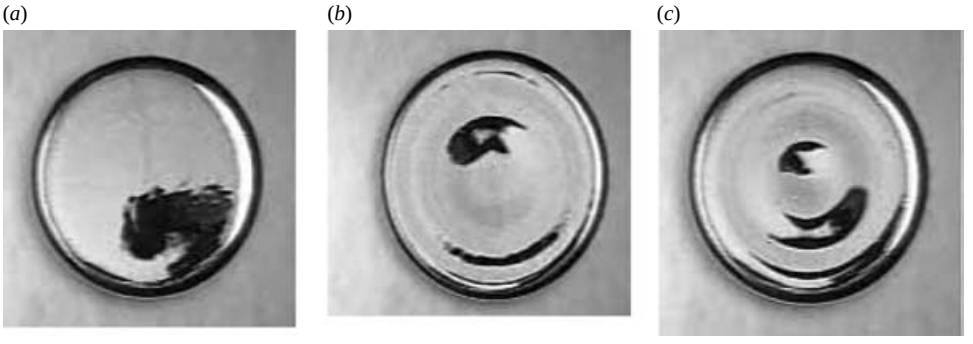

FIGURE 4. Free-surface patterns viewed from above in the first regime for various magnetic field frequencies. The photographs show the modes resulting from the applied frequencies. The oscillation frequency is equal to twice that of the magnetic field (forced-wave regime). The initial drop radius is $a = 30$ mm. The proportionality factor between the magnetic field strength (maximum value in tesla) and the coil current I (r.m.s. value in amperes) is 0.0024. (*a*) $I = 0$. (*b*) $f = 1.354$ Hz, $I = 65$ A. (*c*) $f = 9.602$ Hz, $I = 62$ A.

value is of the same order of magnitude as the estimate of the electromagnetic force (12). This indicates that gravity forces probably play a non-negligible role.

4. Results

In the present experiments, the parameter space mainly consists of three quantities, namely:

(i) the pool radius a;
(ii) the magnetic field strength B_0 or equivalently the coil current I;
(iii) the magnetic field frequency f or angular frequency $\omega = 2\pi f$.

4.1. *Surface patterns*

For a given magnetic field frequency, we increase the magnetic field strength from zero to approximately 0.3 T. Two pool radii are considered, namely $a = 30$ (figures 4–6) and 53 mm (figures 7 and 8). From the observations, three main flow patterns may be distinguished.

Axisymmetric regime

For weak magnetic field values, the free-surface pattern consists of axisymmetric waves, as shown in figure 4. Their frequency is equal to the oscillation frequency of the electromagnetic forces (twice the frequency of the magnetic field), and their deformation is mainly vertical, except in the very low-frequency cases ($f \leqslant 1$ Hz). Their amplitude has not been measured precisely. From side photographs, we observe that the amplitude of the vertical deformation is, at most, of the order of 0.5 mm in the current range considered in this regime. These waves form as soon as the magnetic field strength is non-zero. They are probably directly forced by the oscillating part of the electromagnetic forces in analogy with GF92 and GFS92.

Structured azimuthal waves

When the magnetic field value reaches a given threshold, non-symmetric surface waves appear (figure 5). The wave shape is regular and the wave pattern may be clearly identified. The dominant azimuthal mode, which is excited, depends on the frequency of the magnetic field. Its wavelength decreases as the magnetic field

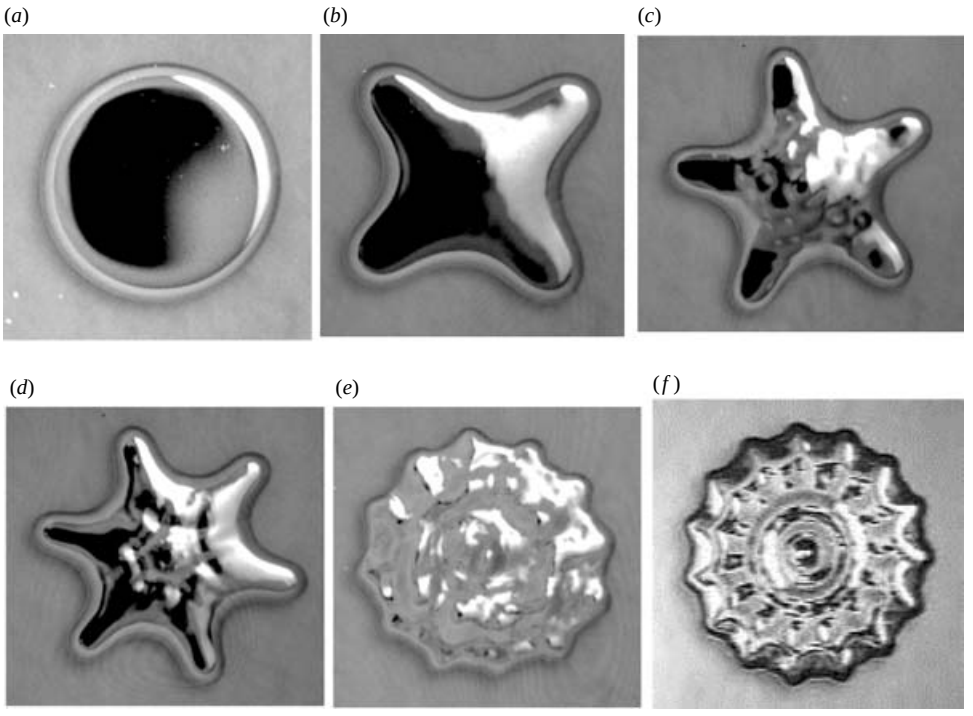

FIGURE 5. Free-surface patterns viewed from above for various magnetic field frequencies. The photographs show the modes resulting from the applied frequencies. The oscillation frequency is equal to that of the magnetic field (parametric regime). The initial drop radius is $a = 30$ mm. The proportionality factor between the magnetic field strength (maximum value in tesla) and the coil current I (r.m.s. value in amperes) is 0.0024. (*a*) $f = 0$ Hz, $I = 0$ A; (*b*) 1.200 Hz, 130 A; (*c*) 1.779 Hz, 7.7 A; (*d*) 2.102 Hz, 103 A; (*e*) 6.205 Hz, 82 A; (*f*) 9.602 Hz, 65 A.

frequency increases. The observed wave frequency is equal to the frequency of the magnetic field (half that of the Lorentz forces), similar to observations in GF92 and GFS92. This type of behaviour is analogous to that encountered in parametric instabilities.

We checked that the pool motion was almost two-dimensional. The whole area of the pool is almost conserved, its variation being less than 10 %. However, the free surface still exhibits vertical forced waves, which are superimposed on the horizontal motion. These waves are responsible for the 'granulation' of the free surface, which is clearly visible in figures 5(*e*) and 5(*f*).

Unstructured regimes

For high values of the coil current, we observe the appearance of unstructured regimes. Such patterns are illustrated in figures 6, 7 and 8. Two pool radii have been used, namely $a = 30$ mm (figure 6) and $a = 53$ mm (figures 7 and 8).

For $a = 30$ mm, pulsating 'fingers' are observed (figure 6). As opposed to the structured regime, the fingers are not organized in a uniform pattern. Although the spatial location of the fingers is random, their motion follows a period of time that is close to the applied magnetic field oscillation period. Thus, the dominant frequency of the whole phenomenon is equal to the magnetic field frequency. For high elongation of a finger, mercury drops are sometimes ejected and then recaptured by the liquid fingers.

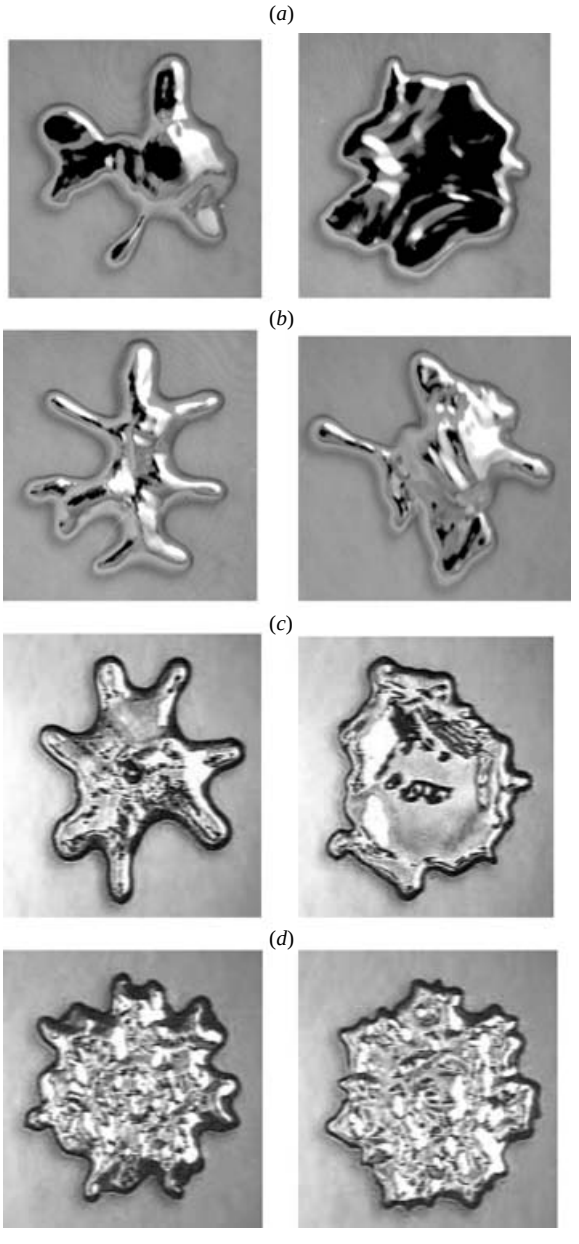

FIGURE 6. Free-surface patterns for various coil frequencies and currents. The initial drop radius is $a = 30$ mm. The photographs show two different instants for identical electric conditions. The proportionality factor between the magnetic field strength (maximum value in tesla) and the coil current I (r.m.s. value in amperes) is 0.0024. (*a*) $f = 1.540$ Hz, $I = 178$ A; (*b*) 2.012 Hz, 175 A; (*c*) 2.399 Hz, 185 A; (*d*) 8.050 Hz, 165 A.

In the case of large pool radius, i.e. $a = 53$ mm, the fingers are once again present, but may be very long. The free-surface pattern exhibits additional features. In figure 7, for example, large intermittent cavities may be observed in the sequence of photographs. A large cavity is formed on the left-hand part of the figure and disappears after approximately 1 s. The cavity is generally associated with a significant horizontal

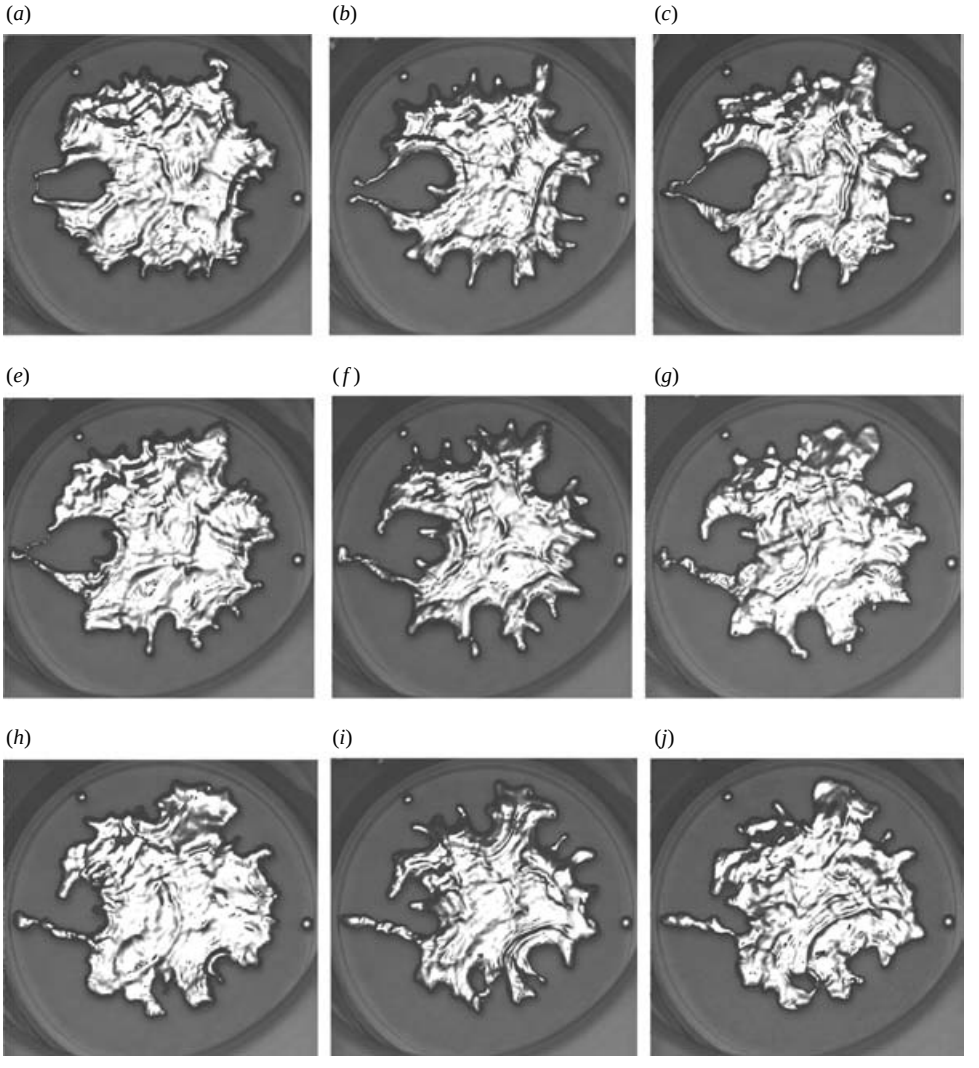

FIGURE 7. Successive views of an unstructured pattern for $f = 4.167$ Hz, $I = 120$ A. The initial drop radius is $a = 53$ mm. The time-interval between each photo is $1/25$ s. Large cavities are visible, for example on the left-hand side. A 'void' inclusion may also be observed in the bottom part of the pool.

rotational motion of the liquid metal in its vicinity. In the same figure, note the development of a similar structure at the bottom of the pool. However, in this case, the cavity is finally closed by a liquid finger (figure 7*i*). This leads to a void inclusion. Such a void inclusion is also observed in figure 8(*a*).

When the coil current becomes even higher, the free surface becomes highly unstructured (e.g. figure 7). The pool bulk exhibits long and narrow ridges. These striations are a consequence of local vertical deformation of the free surface. These vertical ridges may be interpreted as a measure of the pressure field as in open-channel flow. These structures evoke the hydraulic jump phenomenon, which occurs in open-channel flow when the horizontal velocity exceeds the celerity of the surface waves.

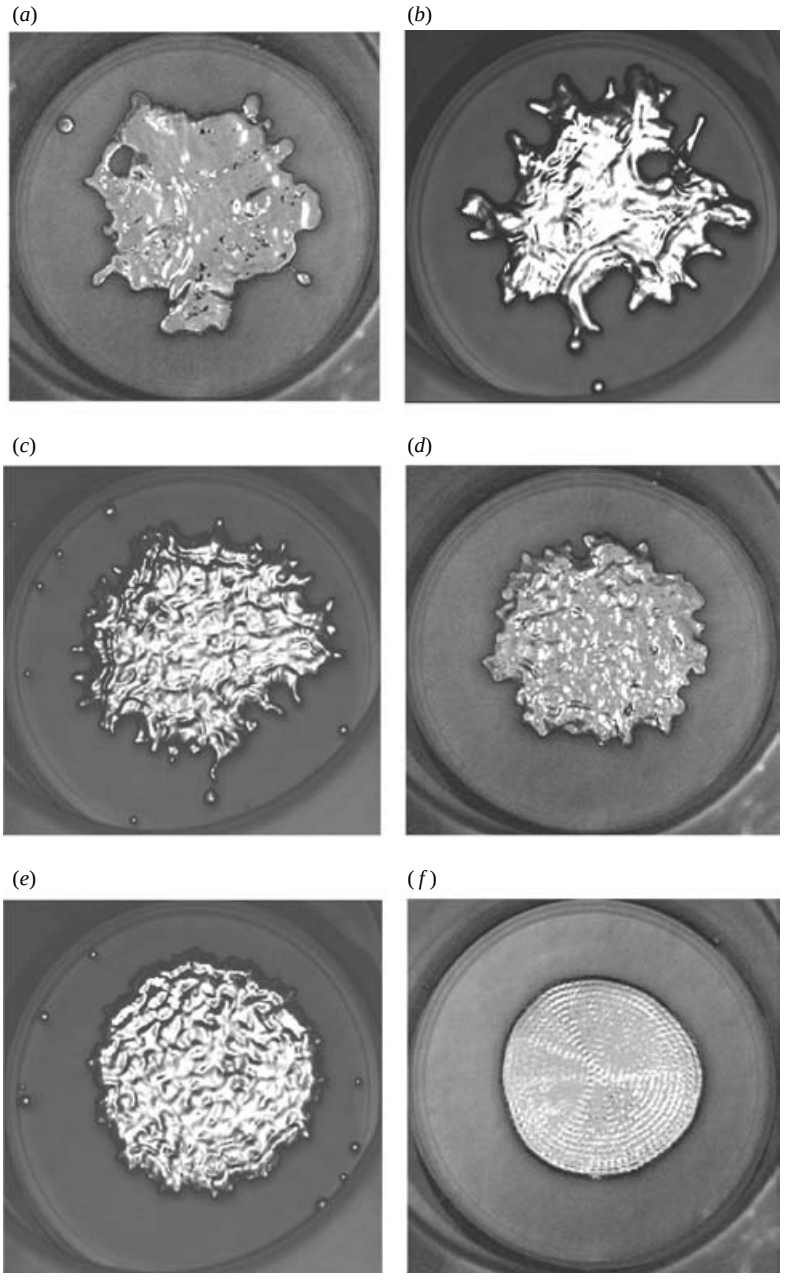

FIGURE 8. Views of non-structured patterns for various frequencies. The initial drop radius is $a = 53$ mm. Note that the length scales decrease as the frequency increases. (*a*) $f = 3.296$ Hz, $I = 124$ A; (*b*) 4.167 Hz, 125 A; (*c*) 7.575 Hz, 125 A; (*d*) 8.106 Hz, 115 A; (*e*) 12.33, 96 A; (*f*) 2.50 Hz, 125 A.

Indeed, the celerity of such waves, which is of the order of $(gh_e)^{1/2} \approx 0.17\,\mathrm{m\,s^{-1}}$, may be less than the liquid velocity estimate given by $\omega\eta_0 \approx 0.26\,\mathrm{m\,s^{-1}}$ for $f = 4.16$ Hz and $\eta_0 = 0.01$ m. As the magnetic field frequency increases, this surface structure disappears and is replaced by a more uniform granulation (figure 8).

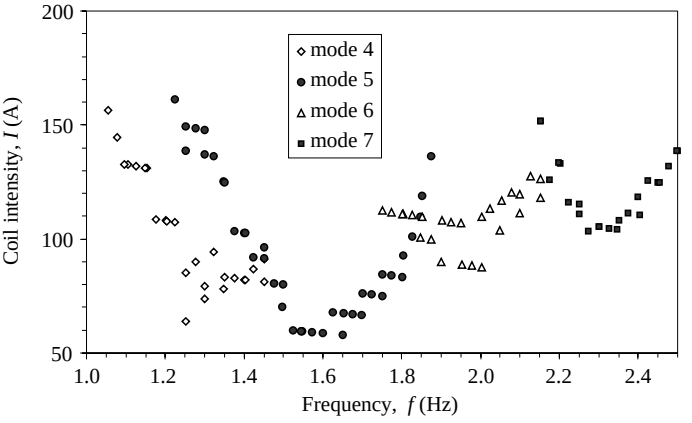

FIGURE 9. Stability boundary of a pool of mercury of 30 mm radius for various magnetic field frequencies. Parametric instability appears as soon the coil current is greater than the threshold value.

As in the previous regime, the length scales of the surface waves decrease as the magnetic field frequency increases. This is clearly visible in figure 8, where the granulation of the pool surface becomes finer and finer as the frequency increases. For the highest frequencies (Figures 8*e* and 8*f*), note that the pool contour is almost smooth in spite of large-scale deformation. Note also that for the configuration shown in figure 8(*f*), the pool is not steady , but slowly moves as a whole toward the side of the substrate.

4.2. *Stability diagram*

Concerning the transition between the axisymmetric and azimuthal regimes, we have determined the threshold value of the magnetic field for various frequencies. We focused on a relatively narrow frequency range between 1 and 2.5 Hz. Beyond $f = 3$ Hz, the determination of the stability thresholds was difficult. Concerning the determination of the threshold value, we observe a strong hysteresis. Thus, all the experimental values given in the stability diagram correspond to increasing values of the coil current I (i.e. increasing magnetic field). The frequency increment is 0.05 Hz. The accuracy for the threshold current is approximately ± 3A. The experimental values are illustrated in the stability diagram of figure 9. Note that the stability curves consist of various narrow 'tongues' of instability each corresponding to an azimuthal mode, i.e. $n = 4, 5, 6, 7$.

For each tongue, we have superimposed various series of measurements in order to test the reproducibility of the experiments. The observations made from these measurements may be summarized as follows:

(i) the odd modes (e.g. $n = 5$ and 7) are easy to trigger as they are more reproducible than even modes;

(ii) the higher the frequency of the magnetic field, the higher the magnetic field amplitude must be to excite parametric waves; a similar phenomenon was observed by GF92;

(iii) the structure of the stability diagram have many similarities with what was observed by GF92 and analysed by GFS92 and, more generally, with the stability diagram of the Mathieu-type equation; this behaviour reinforces the conclusion that the so-called azimuthal waves are a consequence of a parametric-type instability.

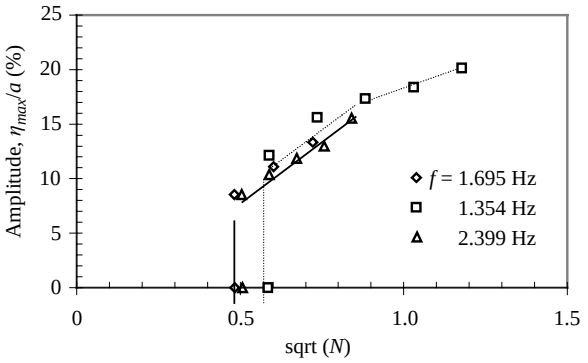

FIGURE 10. Maximal deformation of the horizontal waves normalized by the pool radius versus the square root of the interaction parameter. The data correspond to the structured regime for $a = 30$ mm.

Unstructured regimes appear for higher values of the coil current. It was not possible to determine a stability boundary for this regime. Nevertheless in the case where $a = 30$ mm, it is observed that the number of main 'fingers' is generally close to the mode number which is triggered at the same frequency in the structured pattern. For example, in figure 6(b) (left) the surface pattern comprises approximately six main fingers as in figure 5(d).

4.3. *Wave amplitude*

In the structured regimes, the wave amplitudes have been measured from an analysis of the video recording. For three given frequencies, the maximum horizontal displacement η_{max} is determined as a function of the coil current. We consider only the cases where the motion pattern is structured. The experimental values correspond to an average over ten cycles. We have observed that the experimental data provide a better fit when the dimensionless amplitude is plotted versus the interaction parameter N. The results are shown in figure 10. Owing to the existence of an instability threshold, there are no data for low magnetic field strength, i.e. for approximately $N < 0.2 - 0.3$. We observe that just after the threshold, the wave amplitude increases rapidly to approximately 8 to 10 mm, i.e. 30% of the pool radius. After that, growth is weaker and can be expressed approximately by:

$$\frac{\eta_{max}}{a} = O(N^p) \quad \text{where } p \text{ varies from 0.5 to 0.7.} \tag{14}$$

To interpret this trend, it is of interest to review some theoretical considerations for a case that is geometrically closer to the Faraday experiment (GF92). GF92 have shown that the change in amplitude with respect to the coil current was governed by the following scaling:

(i) linear regime corresponding to small values of N (or weak magnetic field strengths):

$$\frac{\eta_{max}}{a} = O(N), \tag{15}$$

(ii) nonlinear regime corresponding to $N = O(1)$:

$$\frac{\eta_{max}}{a} = O\left(N^{1/2}\right). \tag{16}$$

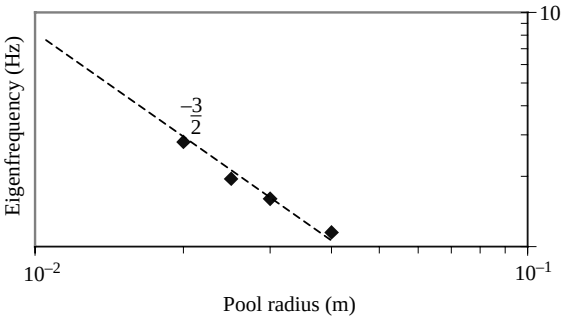

FIGURE 11. Experimental eigenfrequencies versus the pool radius for the mode $n = 5$.

Regarding the experimental results of figure 10, the change in the amplitudes is closer to the estimate given by (16). We may therefore conclude that the observed regimes are probably nonlinear in the parameter range considered here. Note that the growth of the amplitude seems to be weaker for the highest values of N. This can be attributed to the appearance of the Hartmann layer that replaces the viscous boundary layer when $N \geqslant 1$. The oscillation amplitude was not measured for the non-structured regimes. However, the photographs (figures 6–8) show considerable extension of the fingers.

4.4. *Eigenfrequencies*

We compare the experimental pool eigenfrequencies with the theoretical eigenfrequencies, calculated using the two-dimensional approximation (2). The experimental pool eigenfrequencies are determined from the tongue minima shown in figure 9. Such a procedure is only an approximation since nonlinear and viscous effects that could shift the eigenfrequencies are not taken into account. Furthermore, owing to the measurement discrepancies, the minima cannot be determined with great accuracy, especially for the even modes. The data are given in table 3. Note that the experimental eigenfrequencies are qualitatively consistent with the theoretical values, but differ by up to 50% for the highest mode. This may indicate that the motion associated with the dominant mode is not strictly two-dimensional and the small but non-zero vertical displacement is probably responsible for the discrepancy. This argument is consistent with the fact, as explained in § 3, that gravity probably plays as significant a role in the restoring force as the surface tension.

In addition, we have measured the eigenfrequencies of the mode $n = 5$ for various pool radii. The theoretical law (2) derived for the two-dimensional case predicts that the eigenfrequencies f_n vary as:

$$f_n \propto a^{-1.5}. \tag{17}$$

Figure 11 shows that the experimental data do not contradict the scaling (17), but exhibit a slight deviation from the theoretical law (17). Indeed, it is found experimentally that:

$$f_n \propto a^{-1.26}. \tag{18}$$

This indicates, as would be expected, that the surface free modes cannot be described strictly by a two-dimensional approximation.

5. Conclusions

New types of parametric electromagnetic instability have been presented. These instabilities exhibit various horizontal patterns. For low values of the magnetic field, the wave pattern is axisymmetric and the oscillation frequencies are identical to those of the electromagnetic forces. These waves are likely to correspond to forced waves. A similar behaviour was predicted by GFS92. For larger magnetic field amplitudes, the observed waves are structured, but no longer axisymmetric. Their frequency is half that of the Lorentz forces. The corresponding stability diagram presents many similarities with the diagram of the Mathieu–Hill equation, which describes parametric-type instability. This is also supported by the fact that the experimental eigenfrequencies of the liquid pool are comparable to those predicted by the simple two-dimensional model. Thus, the motion is likely to result from a subharmonic transition similar to that proposed by GFS92. For large magnetic field strengths, a peculiar totally chaotic pattern appears, with 'fingers' and cavity formations. Note that the closed cavities correspond to the bubble entrapment mechanism commonly observed in liquid processing.

In our experiments, the appearance of azimuthal waves could be attributed to two possible mechanisms. The first could be related to a destabilization of the forced regime, i.e. the axisymmetric waves, which are directly forced by the magnetic field and are always present. By means of nonlinear interactions, they could lead to a destabilization of the azimuthal modes. This type of nonlinear coupling had been described by Rott (1970) for a double pendulum. Rott demonstrated that the second pendulum (i.e. the azimuthal waves) draws energy from the first pendulum (i.e. the axisymmetric waves) in a periodic exchange. Secondly, the azimuthal system could be triggered directly by a parametric instability, which would be similar to what GFS92 obtained for a horizontal free surface. Indeed, any free-surface horizontal perturbation modifies the horizontal electric current as well and produces a pinching effect in the vicinity of the drop constriction. Accordingly, the electromagnetic force perturbations that are generated reinforce the free-surface deformation until they are balanced by surface tension.

REFERENCES

Batchelor, G. K. 1967 *An Introduction to Fluid Dynamics*. Cambridge University Press.

Daugan, S., Fautrelle, Y. & Etay, J. 1999 Free surface horizontal waves generated by low frequency magnetic field. In *Fluid Flow Phenomena in Metals Processing* (ed. N. El-Kaddah, D. G. C. Robertson, S. T. Johansen & V. R. Voller), pp. 41–48. TMS, Warrendale, PA USA.

Davies, J. T. & Rideal, E. K. 1963 *Interfacial Phenomena*. Academic.

Fautrelle, Y. & Sneyd, A. 1998 Instability of a plane conducting free surface submitted to an alternating magnetic field. *J. Fluid Mech.* **375**, 65–83.

Galpin, J. M. & Fautrelle, Y. 1992 Liquid metal flows induced by low frequency alternating fields. *J. Fluid Mech.* **239**, 383–408.

Galpin, J. M., Fautrelle, Y. & Sneyd, A. 1992 Parametric instability in low frequency magnetic stirring. *J. Fluid Mech.* **239**, 409–427.

Karcher, Ch., Kocourek, V. & Schulze, D. 2003 Experimental investigations of electromagnetic instabilities of free surfaces in a liquid metal drop. *Proc. Intl Scientific Colloquium 'Modelling for Electromagnetic Processing'* (ed. By B. Nacke & E. Baake), pp. 105–110. Institute for Electrothermal Processes, University of Hannover (Germany).

Keizer, J. 1977 Mechanisms of electrochemical oscillations. In *Special Topics in Electrochemistry*, pp. 111–127. Elsevier.

Lamb, H. 1975 *Hydrodynamics* Cambridge University Press.

Li, T., Sassa, K. & Asai, S. 1994 Dynamic meniscus behavior in continuous casting mold with intermittent high frequency magnetic field and surface quality of products. *Proc. Intl Symp. on Electromagnetic Processing of Materials, 25–28 Oct. 1994, Nagoya (Japan), ISIJ*, pp. 242–247.

Miller, C. A. & Neogi, P. 1985 *Interfacial Phenomena.* Marcel Dekker.

Moreau, R. 1990 *Magnetohydrodynamics.* Kluwer.

Padday, J. F. 1969 *Surface and Colloid Sciences*, vol. 1. J. Wiley.

Rott, N. 1970, A multiple pendulum for the demonstration of non-linear coupling. *Z. Angew. Math. Phys.* **21**, 570–582.

Taberlet, E. & Fautrelle, Y. 1985 Turbulent stirring in an experimental induction furnace. *J. Fluid Mech.* **159**, 409–431.

Yoshiyasu, N., Matsuda, K. & Takaki, R. 1996 Self-induced vibration of a water drop placed on an oscillating plate. *J. Phys. Soc. Japan* **65**, 2068–2071.